Antiferromagnetic ordering in the novel $Tb_3Ge_4$ (two-step) and $TbGe_{2-\delta}$ ($AlB_2$-type) compounds studied by neutron diffraction and magnetic measurements



1997 J. Phys.: Condens. Matter 9 9993

(http://iopscience.iop.org/0953-8984/9/45/026)

J. Phys.: Condens. Matter **9** (1997) 9993–10008. Printed in the UK PII: S0953-8984(97)84331-7

# Antiferromagnetic ordering in the novel $Tb_3Ge_4$ (two-step) and $TbGe_{2-\delta}$ ($AlB_2$-type) compounds studied by neutron diffraction and magnetic measurements

O Oleksyn†‖, P Schobinger-Papamantellos†, C Ritter‡, Y Janssen§, E Brück§ and K H J Buschow§

† Laboratorium für Kristallographie, ETHZ, CH-8092 Zürich, Switzerland

‡ Institut Laue-Langevin, 156X, 38042 Grenoble Cédex, France

§ Van der Waals–Zeeman Institute, University of Amsterdam, 1018 XE Amsterdam, The Netherlands

Received 15 May 1997, in final form 8 August 1997

**Abstract.** The magnetic ordering of the novel binary compound $Tb_3Ge_4$ with two Tb sites ($Er_3Ge_4$ structure type, space group $Cmcm$) has been studied by neutron diffraction and magnetic measurements. $Tb_3Ge_4$ orders antiferromagnetically in two steps. In a first step the $Tb_1$ sublattice orders below $T_N = 28$ K with a collinear moment arrangement along the shortest axis $\boldsymbol{a}$ which persists down to $T_1 = 16.5$ K. Below $T_1$ a reorientation of the $Tb_1$ moments takes place. Simultaneously the $Tb_2$ moments order with a collinear arrangement along $\boldsymbol{c}$.

The ordering of the $Tb_1$: 8(f) and $Tb_2$: 4(c) sites is associated with the wavevector $\boldsymbol{q} = (010)$ and is described by the monoclinic magnetic space group $Cp11\frac{2'_1}{m}i'(Sh_{11}^{55})$. At 1.4 K the ordered moment values of $Tb_1$ and $Tb_2$ are 8.4(2) $\mu_B$/atom and 6.3(2) $\mu_B$/atom, respectively. The $Tb_1$ moment is tilted away from the $x$-direction by an angle of 41(2)° and by 57(1)° from the $y$-direction within the $(0yz)$ plane. The resulting structure corresponds to a three-dimensional canting with six sublattices.

The presence of diffuse scattering in the 16.5–53 K temperature interval is attributed to short-range ordered magnetic domains of the mean correlation length ∼11.4(2) Å. Fourier analysis of the data reveals that the first- (up to 4.5 Å) and third- (6.5–7.5 Å) neighbour correlations are mainly ferromagnetic; the second (4.5–6.5 Å) and fourth (7.5–8.5 Å) ones are antiferromagnetic.

The magnetic ordering of the coexisting novel phase $TbGe_{2-\delta}$ with the $AlB_2$ structure type (space group $P6/mmm$) has been also studied. The Tb moments order antiferromagnetically below $T_N = 25$ K. This collinear moment arrangement is associated with the wavevector $(q = 00\frac{1}{2})$ and is described by the magnetic space group $P_{2c}11\frac{2'}{m'}(Sh_{11}^{56})$. At 1.4 K $\mu_{Tb} = 6.7(2)\ \mu_B$ and is confined to the (001) plane.

## 1. Introduction

The magnetic ordering of the isomorphic $R_3Ge_4$ compounds [1] is of interest as the crystal structure comprises two R sites which may give rise to competing interactions and complex ordering phenomena. The R atoms form trigonal prisms centred by Ge atoms and stacked along the $\boldsymbol{a}$ axis. Within the $(0, y, z)$ plane adjacent prisms along $\boldsymbol{b}$ or $\boldsymbol{c}$ are shifted by $x = \frac{1}{2}$ (see section 4.3).

Recently a study of the magnetic ordering of $Er_3Ge_4$ and $Dy_3Ge_4$ compounds [2, 3] was performed. The two Er sublattices order simultaneously below $T_N = 7.3$ K with a triangular

‖ On leave from the Institute of Inorganic Chemistry, Lviv State University, Lviv, Ukraine.

0953-8984/97/459993+16$19.50  

antiferromagnetic moment arrangement within the $(0,\ y,\ z)$ plane. Adjacent prisms display different chiralities. The $Er_1$ magnetic moments make an angle of $35.5(3)^\circ$ with the $y$-direction in the $(0,\ y,\ z)$ plane. The $Er_2$ moments are confined to the $z$-direction over the whole magnetically ordered interval while a reorientation of the $Er_1$ moments sets in at 4 K without any change in symmetry (the magnetic space group $Cp\frac{222'_1}{m'cm}i'(Sh^{391}_{57})$).

$Dy_3Ge_4$ [3] displays a two-step antiferromagnetic ordering associated with a symmetry reduction. The two Dy sites order independently with two distinct order parameters. Each sublattice has a uniaxial antiferromagnetic moment arrangement but different orientations. $Dy_1$ orders below $T_N = 19$ K with the moments along the $\boldsymbol{a}$ axis while $Dy_2$ orders below $T_i = 6$ K perpendicular to $Dy_1$ and is confined to the $\boldsymbol{c}$ axis. In the low-temperature region (LT) the structure is described by the monoclinic magnetic space group $Cp11\frac{2'_1}{m}i'(Sh^{55}_{11})$.

In both cases the antiferromagnetic structures are the result of a strong magnetocrystalline anisotropy and of the presence of competing intrasite $I_{AA}$, $I_{BB}$ and intersite $I_{AB}$ interactions.

In the present investigation we will report on the magnetic ordering of the $Tb_3Ge_4$ compound.

## 2. Sample preparation

The polycrystalline sample of composition $Tb_3Ge_4$ was prepared by arc melting of the elements in an atmosphere of purified argon gas. The purity of the starting materials was 99.9% for Tb and 99.99% for Ge. After arc melting the sample was vacuum annealed at the temperature of 800 °C for three weeks and subsequently quenched in water. The purity of the sample was examined by x-ray powder diffraction. The sample contained a small amount of additional phases.

## 3. Magnetic measurements

Magnetic measurements were made with a SQUID magnetometer. The temperature dependence of the reciprocal susceptibility is shown in figure 1 (top part). Curie–Weiss behaviour is followed down to about 25 K. From the slope and the intercept with the horizontal axis we derive the values $\mu_{eff} = 9.76\ \mu_B$/Tb and $\theta_P = -22$ K for the effective moment and the asymptotic Curie temperature, respectively. The former value is close to the free ion value ($9.72\ \mu_B$/Tb). The temperature dependence of the magnetization, also shown in figure 1 (top part), is characterized by an antiferromagnetic-type transition at about 14 K. The low-temperature behaviour of the magnetization is displayed in more detail in figure 1 (middle part). These data show that there are actually two magnetic phase transitions, occurring at $T_1 = 14.5$ K and $T_N = 26$ K. The field dependence of the magnetization at 5 K is shown in figure 1 (bottom part). In the low-field range the magnetic isotherm at 5 K is characteristic of antiferromagnetic behaviour. There is a change in slope at about 2.8 T, indicative of a field-induced magnetic moment rearrangement. The moment reached in the highest field applied corresponds to $7.0\ \mu_B$ per formula unit or to $2.3\ \mu_B$/Tb.

## 4. Neutron diffraction

Neutron diffraction experiments were carried out at the facilities of the ILL reactor (Grenoble) D1B diffractometer ($\lambda = 2.52$ Å). The data (figure 2) were collected in the

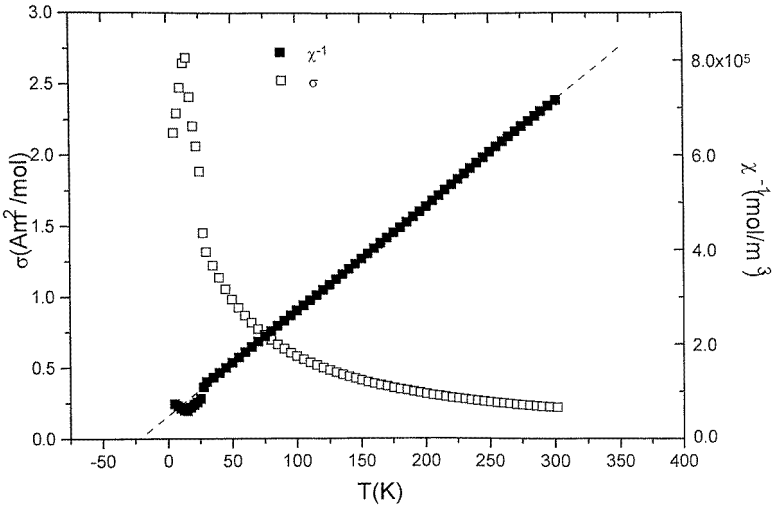


(*a*)

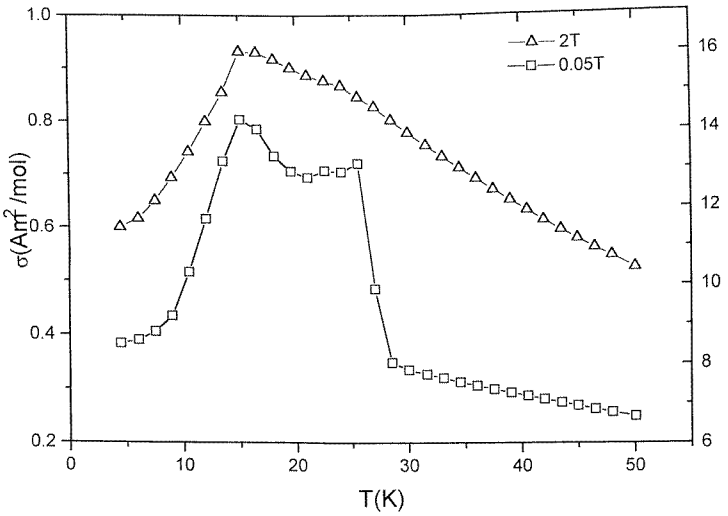


(*b*)

**Figure 1.** Temperature dependence of magnetization of $Tb_3Ge_4$ measured in a field of 2 T (left scale) and of the reciprocal susceptibility (right scale) (*a*). Thermal evolution of the magnetization of $Tb_3Ge_4$ measured in a field of 2 T (right scale) and in a field of 0.05 T (left scale) (*b*). Field dependence of the Tb magnetic moment measured at 5 K (*c*).

temperature range 1.4–92 K with an increment in temperature of 0.5 K. The step increment in $2\theta$ was 0.2°. The data analysis was performed by the Fullprof program [4].

### *4.1. Crystal structure of $Tb_3Ge_4$ and secondary phases*

The neutron patterns in the paramagnetic state confirm the crystal structure of $Tb_3Ge_4$ as reported in [1]. Next to the main contributions of $Tb_3Ge_4$ additional foreign lines were

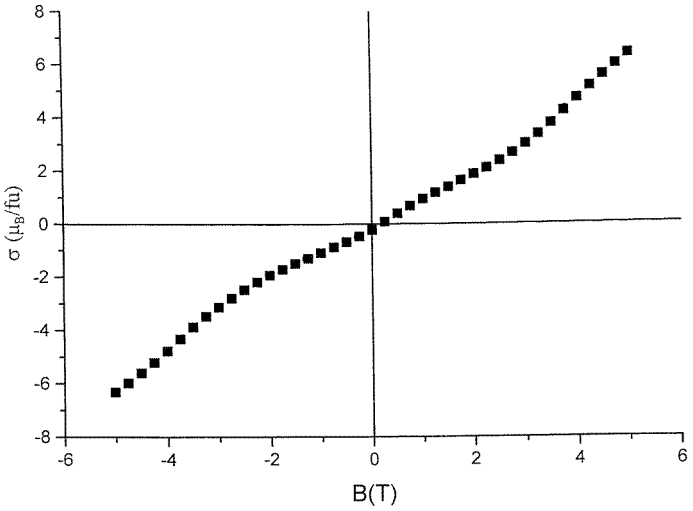


(*c*)

**Figure 1.** (Continued)

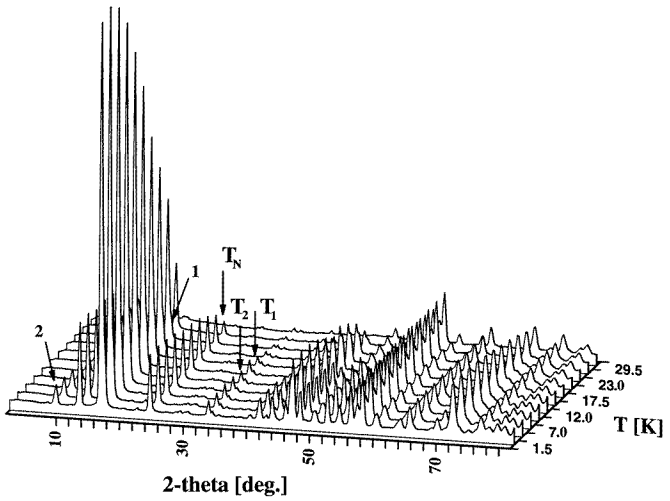


**Figure 2.** A three-dimensional view of the onset of magnetic order in $Tb_3Ge_4$. Selected neutron patterns collected with the D1B spectrometer for 1.4 K $< T \leqslant$ 30 K and $4^\circ < 2\theta < 83.8^\circ$. The strongest magnetic lines of impurity phases are marked by arrows (1—$TbGe_{2-\delta}$, 2—$Tb_5Ge_4$).

detected. The synthesis of a pure sample was seriously hindered by the peritectoid way of formation of $Tb_3Ge_4$.

The foreign lines were identified as a nonstoichiometric phase $TbGe_{2-\delta}$ with the $AlB_2$ structure type [5, 6] which apparently is adjacent to $Tb_3Ge_4$ in the phase diagram.

Below 85 K the patterns comprise an additional contribution in the low-theta region ($2\theta = 9.8^\circ$). This line was attributed to the magnetic ordering of the $Tb_5Ge_4$ phase ($Sm_5Ge_4$ structure type, $T_N = 85$ K: the magnetic structure was reported in [7]). The refined amount of this phase is less than 1%. Due to the very strong intensity of the magnetic (010) line

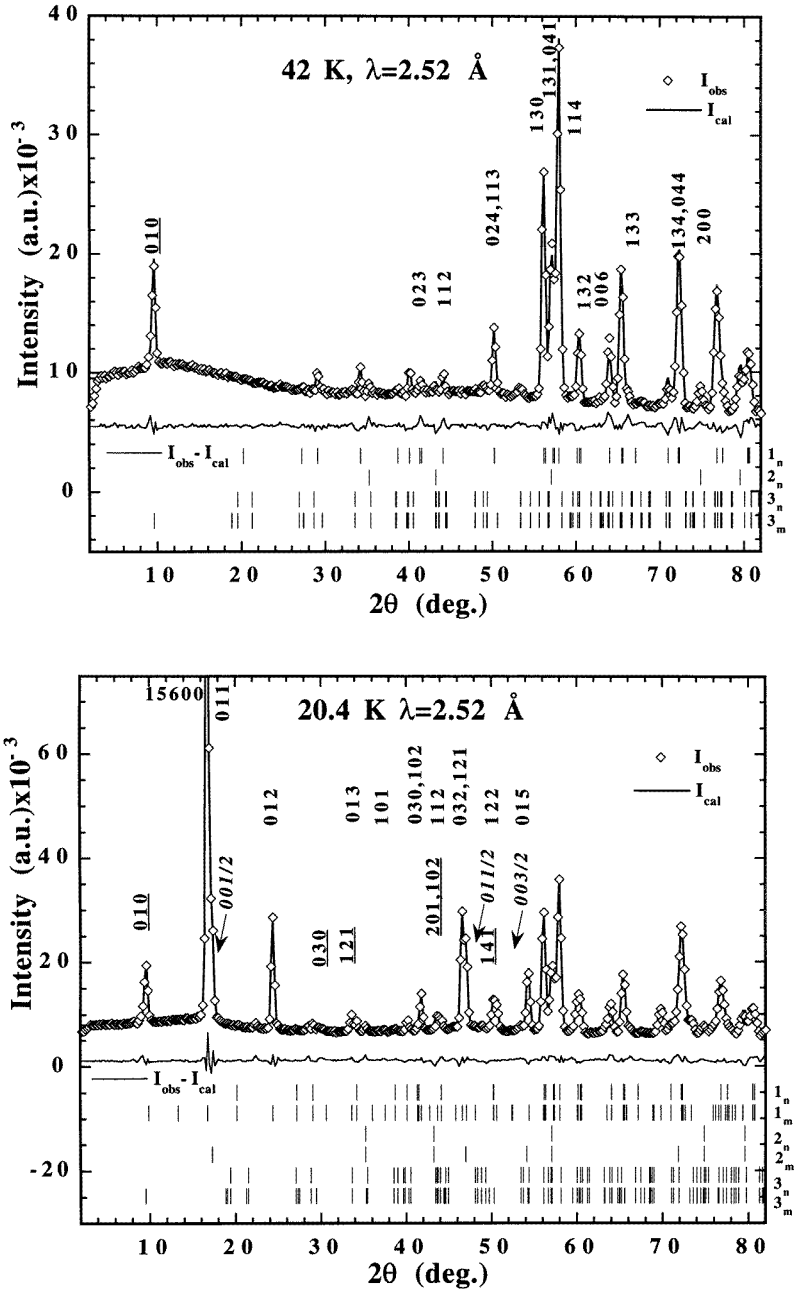


**Figure 3.** Observed, calculated and difference neutron diagram at 42 K (top part), at 20.4 K (middle part) and 1.4 K (bottom part). Six sets of reflections labelled by $1_n$, $1_m$, $2_n$, $2_m$, $3_n$, $3_m$ in the right margin correspond to nuclear and magnetic contributions of $Tb_3Ge_4$, $TbGe_{2-\delta}$ and $Tb_5Ge_4$, respectively. Main magnetic contributions of $Tb_3Ge_4$ are indexed in bold, $TbGe_{2-\delta}$ in italic letters and arrows, indexing of $Tb_5Ge_4$ is underlined.

(100 times stronger than the main nuclear contribution) this negligible amount of impurity became detectable in the magnetically ordered state.

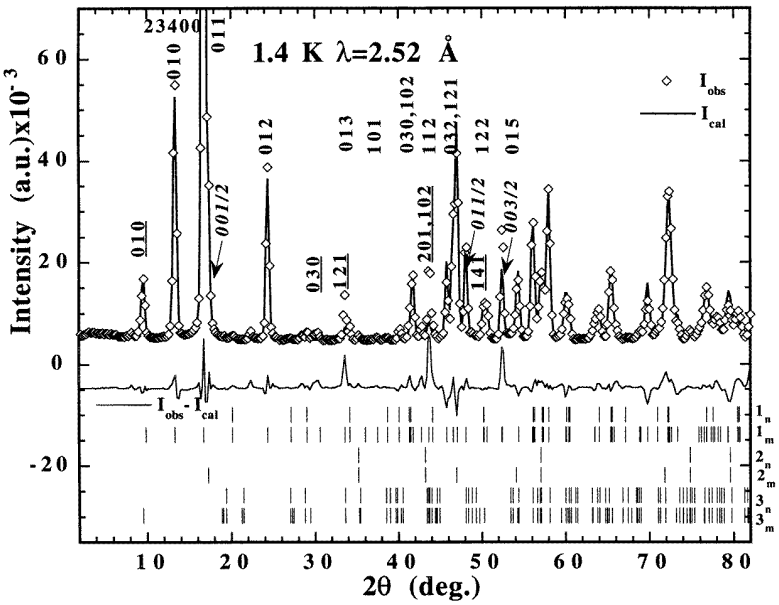


**Figure 3.** (Continued)

Results of the 42 K refinement are displayed in figure 3 (top part) and in table 1. The refinement comprises the coexisting $TbGe_{2-\delta}$ (see section 4.7) and $Tb_5Ge_4$ phases (the latter nuclear and magnetic).

### *4.2. The high-temperature magnetic ordering of $Tb_3Ge_4$ in the range $T_1$–$T_N$*

The magnetic order of the major phase $Tb_3Ge_4$ sets in below $T_N = 28$ K (figure 2). The magnetic reflections occur at reciprocal lattice positions that do not obey the C-centring condition, leading to the anticentred magnetic $C_P$ lattice $\boldsymbol{q} = (010)$. The topology and the relative intensities of the magnetic reflections over the high-temperature (HT) interval $T_1$–$T_N$ ($T_1 = 16.5$ K see section 4.5) are very similar to that observed in the HT interval for $Dy_3Ge_4$ [3]. We therefore used the HT $Dy_3Ge_4$ collinear antiferromagnetic model with the $R_1$ at 8(f): ((1): $(0,\ y,\ z)$, (2): $(0,\ -y,\ \frac{1}{2}+z)$, (3): $(0,\ y,\ \frac{1}{2}-z)$, (4): $(0,\ -y,\ -z)$)+($\frac{1}{2}$, $\frac{1}{2}$, 0)) moments arranged along the $x$-direction. The atoms (1) and (2) related by the $2_{1z}$ rotation are coupled ferromagnetically while the atoms (1) and (3), and (1) and (4) related by the $2_y$ and $2_x$ rotations respectively are coupled antiferromagnetically; the $C_P$ antitranslation reverts the signs. This arrangement is described by the mode $C_x$–$C_x$ $(++---++)$ in the notation of [8] and remains invariant under the transformations of the magnetic space group $Cp\frac{2'22'_1}{mc'm}i'(Sh^{414}_{59})$. The refinement of the magnetic intensities confirms the correctness of the used model (figure 3 middle part, table 1).

### *4.3. Magnetic structure of $Tb_3$ $Ge_4$ at 1.4 K*

At temperatures below $T_1$ (LT region) the topology and relative intensities of the magnetic reflections are modified (see figure 4). The most characteristic feature of the LT patterns is the appearance of the (010) line at $2\theta = 13.6^\circ$. This reflection suggests an ordering of

**Table 1.** Refined parameters from neutron data of $Tb_3Ge_4$ (space group $Cmcm$): (a) at 42 K (paramagnetic state), (b) at 20.4 K in the magnetically ordered HT region (magnetic space group $C_P\frac{2'22'_1}{mc'm}i'(Sh^{414}_{59})$), (c) at 1.4 K in the magnetically ordered LT region (magnetic space group $C_P11\frac{2'_1}{m}i'(Sh^{55}_{11})$) and of $TbGe_{2-\delta}$ (space group $P6/mmm$, magnetic space group $P_{2c}11\frac{2'}{m'}(Sh^{56}_{11})$).

| | 42 K | | 20.4 K | | 1.4 K | |
|---|---|---|---|---|---|---|
| | $y$ | $z$ | $y$ | $z$ | $y$ | $z$ |
| $Tb_3Ge_4$ | | | | | | |
| $Tb_1$ 8f: (0, $y$, $z$) | 0.332(1) | 0.097(1) | 0.3318(5) | 0.095(4) | 0.331(2) | 0.094(1) |
| $Tb_2$ 4c: (0, $y$, $\frac{1}{4}$) | 0.051(2) | 0.25 | 0.047(3) | 0.25 | 0.025(3) | 0.25 |
| $Ge_1$ 8f: (0, $y$, $z$) | 0.375(2) | 0.8878(7) | 0.376(2) | 0.888(2) | 0.391(4) | 0.891(2) |
| $Ge_2$ 4c: (0, $y$, $\frac{1}{4}$) | 0.773(1) | 0.25 | 0.772(2) | 0.25 | 0.765(5) | 0.25 |
| $Ge_3$ 4a: (0, 0, 0) | 0.0 | 0.0 | 0.0 | 0.0 | 0.0 | 0.0 |
| $\mu_{1T}$ [$\mu_B$], $\mu_{2z}$ [$\mu_B$] | | | 6.78(3) | — | 8.4(2) | 6.3(2) |
| $a$, $b$, $c$ [Å] | 4.049(8), 14.222(3) | 10.637(2), | 4.0454(4), 14.218(2) | 10.633(1), | 4.0460(8), 14.207(3) | 10.634(3), |
| $R_n$%, $R_m$% | 5.6, — | | 3.9, 2.1 | | 5.7, 7.9 | |
| $R_{wp}$%, $R_{exp}$% | 11.0, 4.1 | | 9.1, 2.3 | | 17.3, 1.6 | |
| $TbGe_{2-\delta}$ | | | | | | |
| Tb 1a: (0, 0, 0) $\mu_x$ [$\mu_B$] | | | 5.45(8) | | 6.7(2) | |
| Ge 2d: (1/3, 2/3, 1/2) | | | | | | |
| $a$, $c$ [Å] | 3.931(1), | 4.137(2) | 3.9287(8), | 4.1354(4) | 3.928(2), | 4.1337(8) |
| $R_n$%, $R_m$% | 6.0, — | | 7.1, 4.1 | | 8.1, 5.8 | |

the $Tb_2$ moments and/or a canting of the $Tb_1$ moments away from the $x$-direction. The HT magnetic space group $C_P\frac{2'22'_1}{mc'm}i'$ does not allow any mode for the 4(c) site and no other moment component but $\mu_x$ for the 8(f) site (see table 2 in [2]), so a symmetry lowering is obvious.

The 1.4 K refinement has converged for a model (figure 4(a)) which comprises a collinear ordering of $Tb_2$ and a three-dimensional (3D) canting of the $Tb_1$ moments. The arrangement of the $Tb_2$ moments is described by the mode $A_z$–$A_z$ $(+--+)$ in the magnetic space group $C_P\frac{22'2'_1}{m'cm}i'(Sh^{391}_{57})$. The 3D antiferromagnetic $Tb_1$ arrangement has a coupling of the same modes $C_x$–$C_x$, $C_y$–$C_y$ $(++----++)$ along the $x$-, $y$-directions and of the mode $A_z$–$A_z$ $(+--+-++-)$ along the $z$-direction and remains invariant under the transformations of the monoclinic magnetic space group $C_P11\frac{2'_1}{m}i'(Sh^{55}_{11})$.

The ordering of the two Tb sites is described by different magnetic space groups: $Tb_1$ has $C_P\frac{22'2'_1}{m'cm}i'(Sh^{391}_{57})$ symmetry, while $Tb_2$ has $C_P11\frac{2'_1}{m}i'(Sh^{55}_{11})$. The resulting magnetic space group, being the intersection of the two individual groups, coincides with the latter.

The structure comprises six magnetic sublattices (figure 4(b)). The two $Tb_2$ sublattices ($Tb_{21}$ and $Tb_{22}$) are oriented antiferromagnetically along the $z$-direction. The four $Tb_1$ sublattices ($Tb_{1i}$, $i = 1, 4$) are tilted away from the $x$-direction by an angle of $41(2)^\circ$ in four symmetry constrained directions: $\phi_x$, $-\phi_x$, $180 - \phi_x$ and $180 + \phi_x$, respectively. A similar relation holds for the moment angle with the $y$-axis $\phi_{yz} = 57(1)^\circ$ in the $(0, y, z)$ plane (see figure 4(b)). The resulting structure can be described as noncollinear interpenetration of three pairs of collinear sublattices ($Tb_{21}$/$Tb_{22}$, $Tb_{11}$/$Tb_{14}$ and $Tb_{12}$/$Tb_{13}$). The $C_P$ antitranslation and i′ anticentre retain the zero net magnetization of each sublattice.

The low reliability factors $R_n = 5.7\%$, $R_m = 7.9\%$ (see table 1) between the experimental and the calculated 1.4 K patterns (figure 3 bottom part) confirm the correctness

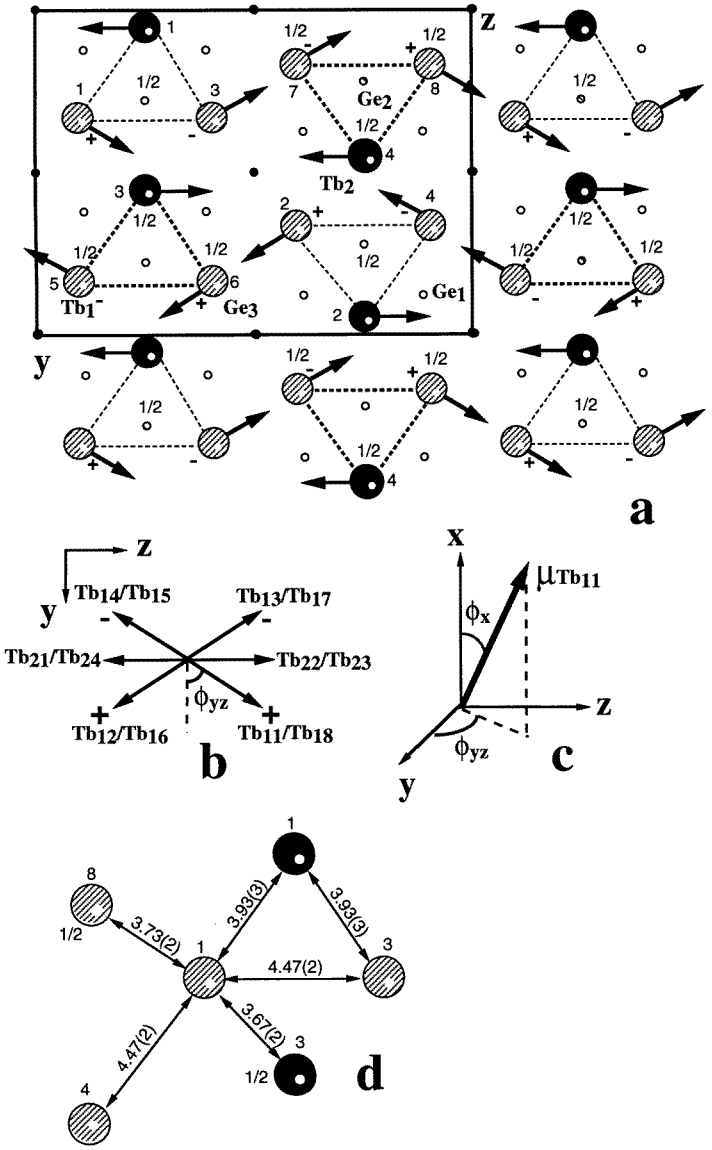


**Figure 4.** Magnetic structure of $Tb_3Ge_4$ in the LT region: (a) projection of the structure along the $x$-axis, (b) mutual orientation of six Tb sublattices along the $x$-axis superimposed into one point, (c) 3D canting of the $\mu_{11}$ moment, (d) typical interatomic Tb–Tb distances.

of the magnetic model proposed. The rather high value of the weighted profile factor $R_{wp} = 17.3\%$ results from the contributions of the secondary phases (mainly $Tb_5Ge_4$). The 1.4 K ordered moment values are $\mu_{2z} = 6.3(2)\ \mu_B$ for $Tb_2$ and $\mu_T = 8.4(2)\ \mu_B$ for the $Tb_1$ site. The former value is considerably lower than the free-ion value of $Tb^{3+}$ ($gJ\ [\mu_B] = 9\ [\mu_B]$).

The arrangement of the $Tb_2$ moments is the same as that of $R_2$ in $Er_3Ge_4$ [2] and in the LT region in $Dy_3Ge_4$ [3]. The similarities in the LT $R_1$ arrangement can preferably

**Table 2.** Coordination shells in $Tb_3Ge_4$. Moment alignment of neighbouring atoms relative to the (1) $Tb_1$ $(0, y, z)$ and (1) $Tb_2$ $(0, y, \frac{1}{4})$ atoms in the LT model is given.

| Shell $N$ | Sign of $g(r)$ | Neighbouring atoms | Tb–Tb distances (Å) | | Sign of the correlation in the LT model | |
|---|---|---|---|---|---|---|
| | | | | | $x$ | $z$ |
| I | + | Tb1–Tb2 | 2 | 3.67(2) | | + |
| | | Tb1–Tb1 | 2 | 3.73(2) | + | + |
| | | Tb1–Tb2 | 1 | 3.93(3) | | − |
| | | Tb1–Tb1 | 2 | 4.044(1) | + | + |
| | | Tb2–Tb2 | 2 | 4.044(1) | | + |
| | | Tb1–Tb1 | 1 | 4.47(2) | + | − |
| | | Tb1–Tb1 | 1 | 4.47(2) | − | − |
| II | − | Tb1–Tb2 | 2 | 5.49(2) | − | − |
| | | Tb1–Tb2 | 2 | 5.64(2) | | − |
| | | Tb1–Tb1 | 4 | 5.69(2) | − | − |
| | | Tb2–Tb2 | 4 | 5.69(4) | | − |
| | | Tb1–Tb1 | 2 | 6.03(2) | − | + |
| | | Tb1–Tb1 | 2 | 6.03(2) | − | − |
| | | Tb1–Tb2 | 1 | 6.16(2) | − | + |
| III | + | Tb1–Tb2 | 2 | 6.79(1) | | + |
| | | Tb1–Tb1 | 2 | 6.83(1) | + | + |
| | | Tb2–Tb2 | 2 | 7.122(4) | | − |
| | | Tb1–Tb1 | 4 | 7.24(2) | + | − |
| | | Tb1–Tb2 | 2 | 7.37(2) | | + |
| IV | − | Tb1–Tb1 | 1 | 7.49(2) | − | − |
| | | Tb1–Tb1 | 4 | 7.58(2) | − | + |
| | | Tb1–Tb2 | 1 | 7.73(3) | | − |
| | | Tb1–Tb2 | 2 | 7.93(1) | | − |
| | | Tb1–Tb1 | 2 | 7.97(2) | + | − |
| | | Tb1–Tb1 | 4 | 8.07(2) | − | − |
| | | Tb2–Tb2 | 4 | 8.07(3) | | − |
| | | Tb1–Tb1 | 2 | 8.089(3) | + | + |
| | | Tb2–Tb2 | 2 | 8.089(3) | | + |
| | | Tb2–Tb2 | 4 | 8.191(3) | | − |
| | | Tb1–Tb2 | 1 | 8.40(3) | | + |
| | | Tb1–Tb1 | 2 | 8.51(2) | − | − |

be followed on the basis of Cartesian coordinates. The $Tb_1$ $x$-component is dominant ($\mu_{1x} = 6.3(2)\ \mu_B$) reminiscent of the HT collinear antiferromagnetic $Tb_1$ arrangement (realised as well in $Dy_3Ge_4$). The moment arrangement within the $(0, y, z)$ plane is similar to that in $Er_3Ge_4$. The only difference consists on the angle $\phi_{yz}$ which is $57(1)^\circ$ for Tb and $35.5(3)^\circ$ for Er.

As will be shown in the next sections this structure is stable only in the LT region up to about 8 K.

### *4.4. Thermal evolution of the three-dimensional canting of $Tb_1$ moments below $T_1$ in $Tb_3Ge_4$*

The thermal evolution of the $Tb_1$ and $Tb_2$ moments below $T_1$ gives a more complete insight into the evolution of the overall magnetic order in $Tb_3Ge_4$. For this purpose we restrict

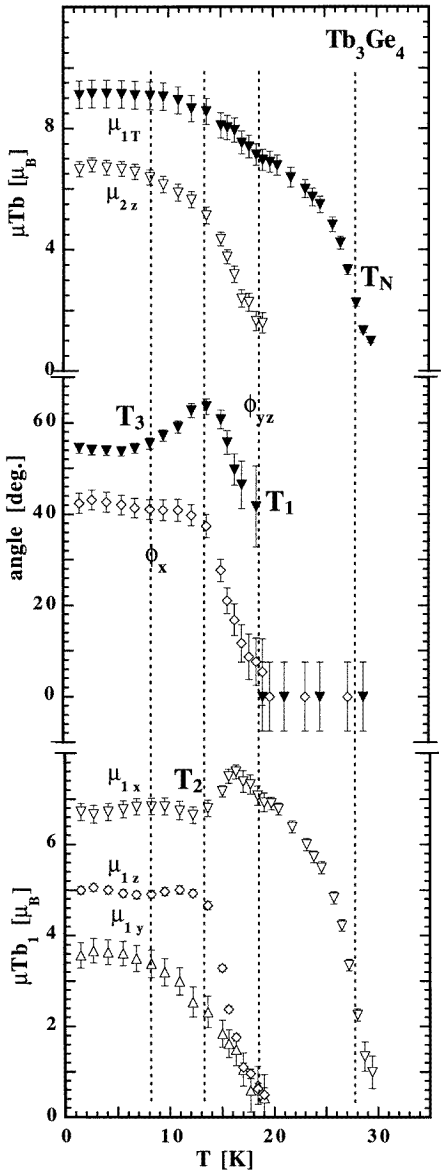


**Figure 5.** Thermal evolution of the magnetic order in $Tb_3Ge_4$. The variation of the total magnetic moments $\mu_{1T}$ and $\mu_{2z}$ of the $Tb_1$ and $Tb_2$ sites (top part). The evolution of the $\phi_x$ (tilt away from the $x$-axis) and the $\phi_{yz}$ (departure from the $y$-axis in the $(0, y, z)$ plane) angles (middle part). The temperature dependence of the $\mu_{1x}$, $\mu_{1y}$ and $\mu_{1z}$ $Tb_1$ components (bottom part).

ourselves to the description of a single sublattice of each site as the other sublattices are symmetry related. In spherical coordinates the spin reorientation transition of the $Tb_1$ moments can be described by the evolution of the total moment value and the tilt of the moment away from the $x$-direction (angle $\theta_x$) and away from the $y$-direction within the $(0, y, z)$ plane (angle $\phi_{yz}$).

The total $Tb_1$ moment value changes rather smoothly with cooling (figure 5, top part) and displays one poorly pronounced singularity at $T_1$.

Concerning the temperature dependent evolution of the $\phi_x$ and $\phi_{yz}$ angles one may distinguish three temperature regions of different behaviour (figure 5, middle part) defined by the points ($T_1$, $T_2$, $T_3$).

In the $T_2$–$T_1$ interval the $Tb_1$ moment deflects progressively from the $x$- and $y$-directions (increasing values of the $\phi_x$, $\phi_{yz}$ angles). Below $T_2 \approx 13$ K $Tb_1$ has reached its saturation value and the angle $\phi_x$ preserves a constant value while the $\phi_{yz}$ angle decreases (figure 5, middle part) and attains a constant value only below $T_3 \approx 8$ K. This means that in the $T_3$–$T_2$ interval the $Tb_1$ moment turns back towards the $y$-direction. In Cartesian coordinates one obtains more details on the nature of the competing interactions (figure 5, bottom part). The $\mu_{1x}$- and $\mu_{1z}$-components are coupled below $T_1$. In the $T_2$–$T_1$ interval $\mu_{1z}$ increases while $\mu_{1x}$ decreases, and both achieve a constant value below $T_2$. The $\mu_{1y}$-component develops independently and increases smoothly with cooling below $T_1$.

The observed thermal behaviour of the $Tb_1$ and $Tb_2$ moments suggests the following evolution of the $Tb_3Ge_4$ magnetic order. In the first step (below $T_N$) $Tb_1$ orders independently with a collinear antiferromagnetic arrangement along the $x$-direction. In the second step (below $T_1$) the ordering of the $Tb_1$ and $Tb_2$ moments is coupled. The $Tb_2$ moments are strictly confined to the $z$-direction. The $Tb_1$ moments reorient away from the $x$-axis starting from the [011] direction and developing towards the $z$-direction with cooling. In simple terms this behaviour might be considered as a field action opposite the line bisecting the angle between the two $Tb_{11}/Tb_{12}$ and $Tb_{13}/Tb_{14}$ sublattices. In the vicinity of $T_2$ however things become more complex as the $Tb_1$ moments are restrained from further rotation towards the $z$-direction. Below $T_3$ the $Tb_1$ and $Tb_2$ moments are close to saturation and the angles $\phi_x$ and $\phi_{yz}$ remain unchanged; the equilibrium between the competing intersite interactions is established.

### *4.5. Thermal evolution of Bragg magnetic intensities of $Tb_3Ge_4$*

Here we would like to note that there is a small discrepancy on the exact values of the transition temperatures extracted on the basis of the refined physical quantities (moment values and angles) as a function of temperature (figure 5) if compared to those extracted from the $T$-dependence of the magnetic intensities (figure 6). This is related to the presence of diffuse scattering in the HT region overlapping with some magnetic intensities which in the former case leads to higher values and larger error limits of the transition temperatures. We therefore consider the values obtained from the integrated intensities as more reliable. Within the error limits these values are in agreement with those obtained from the magnetic measurements (figure 1).

Figure 6 shows the thermal evolution of three selected magnetic integrated intensities extracted by a fitting procedure. The (011) and (032) lines appear below $T_N$ and display slope changes at three distinct temperatures: $T_1 = 16.5$ K, $T_2 = 13$ K and $T_3 = 8$ K. The (010) line arises only at $T_1$; its intensity increases steeply up to $T_2$, remains unchanged in the $T_2$–$T_3$ interval and increases slightly at lower temperatures.

The different thermal behaviour of these reflections originates from the different contributions of the $Tb_1$ and $Tb_2$ moment components into the corresponding structure factors. The structure factor of the (032) reflection has equal contributions of the $\boldsymbol{\mu}_{1x}$ and $\boldsymbol{\mu}_{1y}$ components which add up: $F(032) \sim 4 \times 0.935(\boldsymbol{\mu}_{1x} + \boldsymbol{\mu}_{1y})$. Therefore the corresponding intensity follows the evolution of the dominant $Tb_1$ $x$-component and its reorientation towards the $y$-direction. The (010) reflection comprises contributions of the

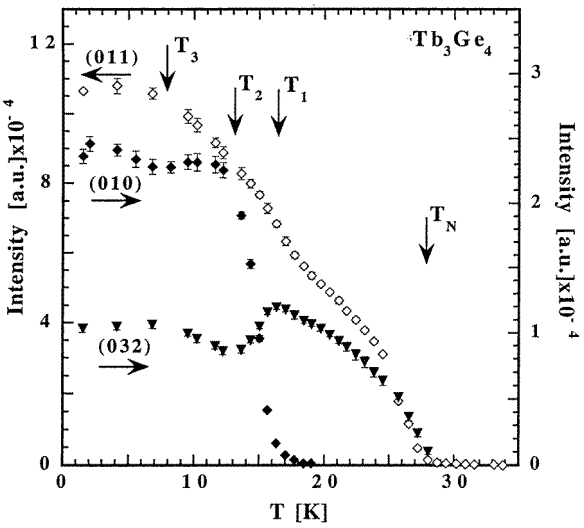


**Figure 6.** Temperature dependence of the magnetic intensity of the (010), (032) and (011) reflections of $Tb_3Ge_4$. Critical temperatures $T_N$, $T_1$, $T_2$ and $T_3$ are detected.

$\boldsymbol{\mu}_{1z}$ and $\boldsymbol{\mu}_{2z}$ components of different sign (the former strongly dominating: $F(010) \sim 2 \times (1.728\boldsymbol{\mu}_{1z} - 0.327\boldsymbol{\mu}_{2z})$. Thus from the evolution of this line the change of the $Tb_1$ and $Tb_2$ $z$-components can be followed. The superposition of all components in the structure factor of the (011) reflection, $F(011) \sim 2 \times (1.428(\boldsymbol{\mu}_{x1} + \boldsymbol{\mu}_{y1}) - 0.566\boldsymbol{\mu}_{z1} + 0.945\boldsymbol{\mu}_{z2})$, leads to the smoothing of the individual magnetic contributions in the (011) intensity.

### *4.6. The short-range magnetic correlations in $Tb_3Ge_4$ in the range 16.5–53 K*

An important feature observed in the neutron data in the range 16.5–53 K is the presence of the broad diffuse humps in the 5–25 and 40–60° $2\theta$ ranges, which correspond to $0.2 < Q < 1.1$ and $1.7 < Q < 2.5$ Å$^{-1}$ ($Q = 4\pi/\lambda \sin\theta$) values. The diffuse scattering is most intense around the (010) and (011) positions ($2\theta = 13.61$ and 17.03°) of the anticentred magnetic $C_P$ lattice of $Tb_3Ge_4$ and appears to be critical in the vicinity of $T_N = 28$ K. In order to separate the magnetic short-range scattering in the low-temperature data sets, the high-temperature (74.5 K) data were subtracted thus removing the nuclear and paramagnetic contributions.

In the $T_1$–$T_N$ interval both the Bragg and the diffuse scattering are visible (figure 7 top part). The diffuse intensity decreases quite slowly with $T$ and vanishes as the temperature approaches $T_1$. These observations suggest that the diffuse scattering is of magnetic origin and corresponds to magnetic correlations with a limited spatial extent.

The inverse full width at half maximum (FWHM in Å$^{-1}$) of the diffuse peaks can be taken as a measure of the mean correlation length $\xi$ ($2\pi$/FWHM) for the short-range magnetic ordering. The Gaussian fit of the diffuse intensity at $T_N$ yields an average correlation length of 11.4(2) Å.

The magnetic diffuse scattering contains information about the magnetic correlations of the neighbouring atoms [9]. However in the particular case of $Tb_3Ge_4$, it was difficult to

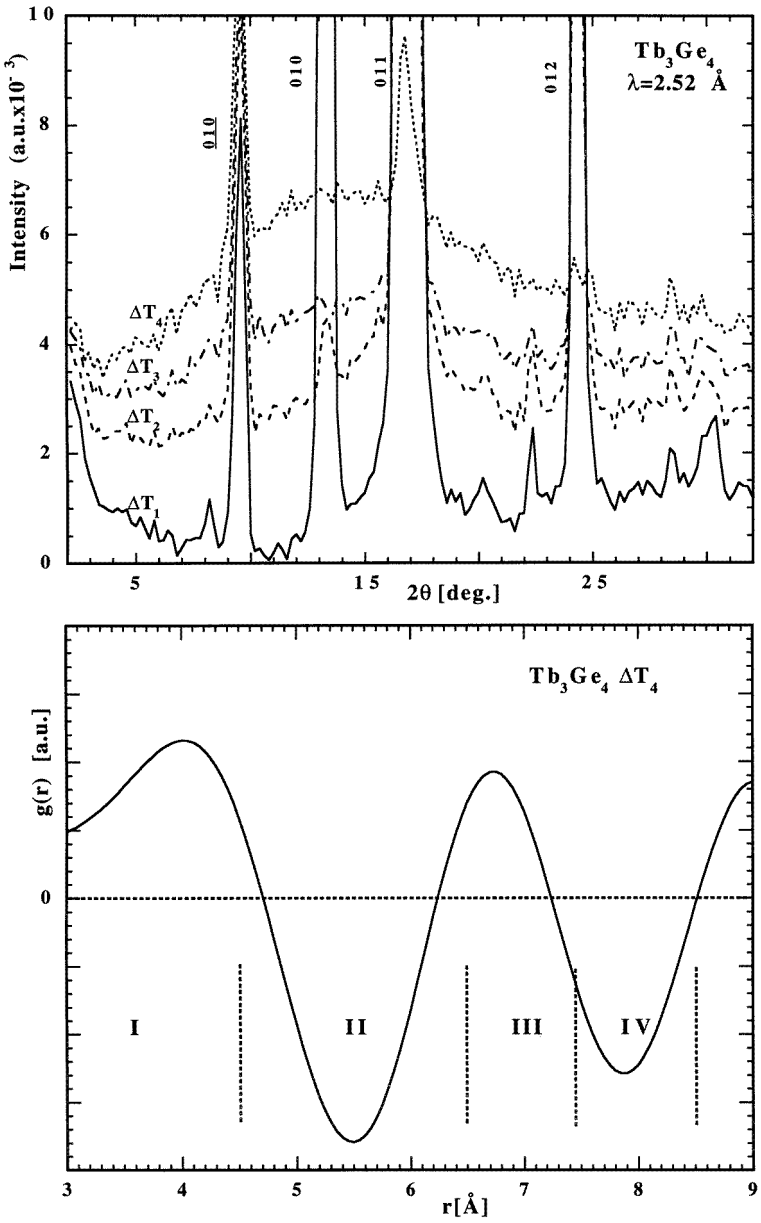


**Figure 7.** Thermal evolution of magnetic diffuse scattering ($\Delta T_1 = 1.4$–74.5 K, $\Delta T_2 = 1.7$–74.5 K, $\Delta T_3 = 23.1$–74.5 K, $\Delta T_4 = 28.7$–74.5 K) (top part). Radial correlation function obtained by Fourier transforming the $\Delta T_4$ data (bottom part).

determine the exact values of the short-range order coefficients due to the complexity of the atomic arrangement. We performed therefore a qualitative estimation assuming only isotropic short-range correlations and using the radial correlation function (equation (1)) as given in [10, 11]. This corresponds to the sum of the moment correlations separated by the

distance $r$ (figure 7, bottom part)

$$g(r) = \int_{Q1}^{Q2} I_{diff}(Q)[f(Q)]^{-2} Q \sin(Qr)\,\mathrm{d}Q \tag{1}$$

where $I_{diff}(Q)$ is the magnetic intensity at $Q$ (the paramagnetic part is subtracted), $f(Q)$ is the Tb magnetic form factor.

The typical interatomic Tb–Tb distances for the $Tb_3Ge_4$ crystal structure are considered (figure 4(d), table 2). As the ordering occurs over a length scale of two or three nearest-neighbour Tb–Tb distances only few nearest coordination shells were examined. In the first and third shells (I: 11 Tb atoms at distances up to 4.5 Å, III: 12 Tb atoms at 6.5–7.5 Å) the ferromagnetic correlations dominate. The second- and fourth-neighbour correlations (II: 17 atoms at 4.5–6.5 Å, IV: 29 atoms, 7.5–8.5 Å) are mostly antiferromagnetic. These findings are consistent with the LT model long-range correlations (see last column in table 2). We infer that some of the magnetic interactions realized in the long-range scale in the LT interval exist in the local scale well above $T_1$.

The preferable direction of these correlations can be guessed from the atomic arrangement and thermal evolution of the magnetic order (sections 4.2–4.5). One of the dominating diffuse features is observed around the (010) position. The (010) Bragg reflection develops in the LT region and comprises contributions only of the $\boldsymbol{\mu}_{1z}$ and $\boldsymbol{\mu}_{2z}$ components. This fact is suggestive of an important $z$-component of the short-range correlations.

One more geometrical factor supports this assumption. Within the HT interval the $Tb_1$ moments have the collinear antiferromagnetic arrangement along the $x$-direction. Since each $Tb_2$ moment is adjacent to four oppositely aligned $Tb_1$ moments (two with $x = 0$ and two with $x = \frac{1}{2}$, see figure 4), it is geometrically frustrated and can order only on a local scale above $T_1$.

### *4.7. Crystal and magnetic structures of $TbGe_{2-\delta}$*

As already mentioned (section 4.1) the 42 K neutron data comprise next to the nuclear reflections of $Tb_3Ge_4$ additional reflections of a novel phase $TbGe_{2-\delta}$ with the $AlB_2$ structure (space group $P6/mmm$). The simultaneous refinement of $TbGe_{2-\delta}$ and $Tb_3Ge_4$ parameters (table 1, figure 3) shows that the amount of the secondary phase does not exceed 12%. According to microspectral analysis the composition of the phase is $TbGe_{2-\delta}$ ($\delta = 0.5$).

In the 1.4 K neutron data additional lines of magnetic origin were observed. They were attributed to the magnetic ordering of $TbGe_{2-\delta}$ and indexed with a $2\boldsymbol{c}$-cell enlargement ($\boldsymbol{q} = 00\frac{1}{2}$) of the chemical unit cell (strong magnetic peaks are indexed in italic in figure 3, bottom part). The topology and the relative intensities are similar to that observed in the isomorphic $TbSi_{1.67-\delta}$ [12] and $DyGe_{1.3(1)}$ [3]. We therefore used the same collinear antiferromagnetic arrangement $(+ - + - \cdots)$ for the Tb (000) magnetic moments perpendicular to the hexagonal axis. This arrangement remains invariant under the transformations of the magnetic space group $P_{2c}11\frac{2'}{m'}(Sh_{11}^{56})$. The agreement between the observed and calculated 1.4 K patterns is quite satisfactory ($R_n = 8.1\%$, $R_m = 5.8\%$). However, a superstructure formation (ordering of Ge defects) or more complex magnetic structure are possible [13].

Figure 8 displays the thermal evolution of integrated intensity of the dominant $(00\frac{1}{2})$ reflection, leading to the ordering temperature of $T_N = 25$ K. At 1.4 K the ordered moment value is $\mu_{Tb} = 6.7(2)\ \mu_B$/Tb.

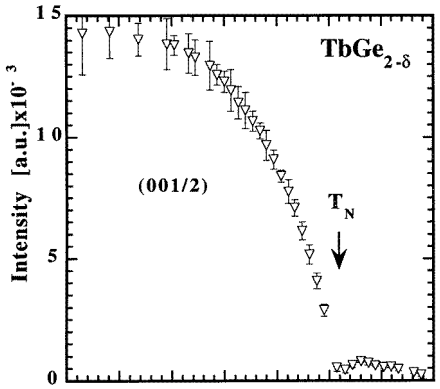


**Figure 8.** Temperature dependence of the $(00\frac{1}{2})$ magnetic intensity of $TbGe_{2-\delta}$ ($AlB_2$ structure).

## 5. Conclusions

The magnetic structures and phase transitions of the novel phases $Tb_3Ge_4$ and $TbGe_{2-\delta}$ were studied in the 1.4–92 K interval by neutron diffraction and magnetic measurements.

$Tb_3Ge_4$ shows a complex two-step magnetic ordering as a consequence of competition of various exchange interactions related to the presence of two Tb positions. The importance of these interactions changes as a function of temperature. Below $T_N$ the intrasite $I_{11}$ interaction is dominant, forcing the $Tb_1$ moments to order with a simple collinear antiferromagnetic arrangement along the $x$-direction indicating a strong anisotropy. This arrangement leads to a geometrical frustration of the $Tb_2$ moments. Presumably above $T_1$ the ordering of $Tb_2$ can be realized only on a local scale (up to $\sim$11 Å) as follows from the observed diffuse magnetic scattering. Below $T_1$ the $I_{11}$ interactions are still important but the intrasite $I_{22}$ and intersite $I_{12}$ interactions start to influence the ordering process. The $Tb_2$ moments order with a collinear antiferromagnetic arrangement along the $z$-direction which is presumably defined by the crystal field. The 3D reorientation of the $Tb_1$ moments is strongly dependent on the $I_{12}$ interaction and the thermal evolution of the crystal-field anisotropy. The $I_{12}$ antiferromagnetic interaction most probably causes the rotation of the $Tb_1$ moments towards the $z$-direction. The equilibrium between the competing intrasite $I_{11}$, $I_{22}$ and intersite $I_{12}$ interactions is established only below $T_3$.

The magnetic ordering of the studied $R_3Ge_4$ compounds (R = Tb, Dy, Er) exhibits a number of common features:

- The moment arrangement within the isolated trigonal prism depends on the R atom while the mutual moment of atoms of the adjacent prisms is constrained by the $C_P$ and i′ symmetry operations.
- The two $R_1$ and $R_2$ sites have different preferred directions of antiferromagnetism and different thermal behaviour.
- The easy axis of antiferromagnetism of the $R_2$ site is along the $z$-direction. At 1.4 K the $R_2$ moment value is reduced compared to the free $R^{3+}$ ion saturation value $gJ\mu_B$ while the moment value of the $R_1$ site attains the free $R^{3+}$ ion saturation value.
- For all three compounds the $I_{11}$ interaction is dominant in the HT region. The intrasite $I_{22}$ and intersite $I_{12}$ interactions become more important at lower temperatures. However the magnitude of these interactions depends on the nature of the R atom.

**Acknowledgments**

This work is financially supported by the Swiss National Foundation, Bern. The authors wish to thank M Honal for help in microspectral analysis.

**References**

[1] Oleksyn O Ya and Bodak O I 1994 *J. Alloys Compounds* **210** 19
[2] Schobinger Papamantellos P, Oleksyn O, Ritter C, de Groot C H and Buschow K H J 1997 *J. Magn. Magn. Mater.* **169** 253
[3] Oleksyn O, Schobinger Papamantellos P, Ritter C, de Groot C H and Buschow K H J 1997 *J. Alloys Compounds* at press
[4] Rodriguez-Carvajal J 1993 *Physica* B **192** 55
[5] Eremenko V N, Meleshevich K A, Buyanov Yu I and Martsenyuk P S 1988 *Soviet Progress in Chemistry, Ukrainskii Khimicheskii Zhurnal* **54** 10
[6] Gladyshevskii E I 1964 *Zh. Strukt. Khim.* **5** 523
[7] Schobinger Papamantellos P 1978 *J. Phys. Chem. Solids* **39** 197
[8] Bertaut E F 1963 *Magnetism* vol 3, ed G T Rado and H Suhl (New York: Academic) ch 4, p 149
Bertaut E F 1975 *Ann. Phys.* **9** 93
[9] Blech I A and Averbach B L 1964 *Phys.* **1** 31
[10] Bertaut E F and Burlet P 1967 *Solid State Commun.* **5** 279
[11] Reimers J N, Greedan J E, Kremer R K, Gmelin E and Subramanian M A 1991 *Phys. Rev.* B **43** 3387
[12] Schobinger Papamantellos P, de Mooij D B and Buschow K H J 1989 *J. Magn. Magn. Mater.* **79** 231
[13] Oleksyn O, Schobinger Papamantellos P, Ritter C and Buschow K H J *Ann. Phys.* at press